Articles

Relationship between the Size of the Bottleneck 15 Å from Iron in the Main Channel and the Reactivity of Catalase Corresponding to the Molecular Size of Substrates‡

Isao Hara,[§,||] Nobutoshi Ichise,[§] Kiyoshi Kojima,[§,⊥] Hidemasa Kondo,[§] Satoru Ohgiya,[§] Hidetoshi Matsuyama,[⊥] and Isao Yumoto*[,§,@]

Research Institute of Genome-based Biofactory, National Institute of Advanced Industrial Science and Technology (AIST), Tsukisamu-Higashi, Toyohira-ku, Sapporo 062-8517, Japan, Department of Bioscience and Technology, School of Engineering, Hokkaido Tokai University, Minaminosawa, Minami-ku, Sapporo 005-8601, Japan, and Graduate School of Agriculture, Hokkaido University, Kita-ku, Sapporo 060-8589, Japan

Received July 28, 2006; Revised Manuscript Received October 27, 2006

ABSTRACT: A catalase that exhibits a high level of activity and a rapid reaction with organic peroxides has been purified from *Exiguobacterium oxidotolerans* T-2-2^T (EKTA catalase). The amino acid sequence of EKTA catalase revealed that it is a novel clade 1 catalase. Amino acid residues in the active site around the protoheme are conserved in the primary structure of EKTA catalase. Although the general interactions of molecules larger than hydrogen peroxide with catalases are strongly inhibited because of the selection role of long and narrow channels in the substrate reaching the active site, the formation rate of reactive intermediates (compound I) in the reaction of EKTA catalase with peracetic acid is 77 times higher than that of bovine liver catalase (BLC) and 1200 times higher than that of *Micrococcus luteus* catalase (MLC). The crystal structure of EKTA catalase has been determined and refined to 2.4 Å resolution. The main channel structure of EKTA catalase is different from those of BLC and MLC. The rate constant of compound I formation in catalases decreased with an increase in the molecular size of the substrate. For EKTA catalase with a larger bottleneck 15 Å from the iron (entrance of narrow channel) in the main channel, a lower rate of reduction in compound I formation rate with an increase in the molecular size of substrates was found. The increase in the rate constant of compound I formation in these catalases was directly proportional to the increase in the size of the bottleneck in the main channel when molecules of substrates larger than H_2O_2, such as organic peroxides, are used in the reaction. The results indicate that the size of the bottleneck in the main channel in catalase is an important factor in defining the rate of compound I formation corresponding to the molecular size of the substrates, and this was demonstrated. The Leu^{149}−Ile^{180} and Asp^{109}−Met^{167} combinations at the entrance of the narrow channel in EKTA catalase determine the size of the bottleneck, and each atom-to-atom distance for the combination of residues was larger than those of corresponding combinations of amino acid residues in BLC and MLC. The combination of these four amino acids is quite specific in EKTA catalase as compared with the combinations in other catalases in the gene database (compared with more than 432 catalase genes in the database).

Catalase (EC 1.11.1.6) protects organisms against oxidative damage by the dismutation of hydrogen peroxide into one dioxygen and two water molecules (*1*). Catalase consists of four identical subunits each equipped with an Fe^{3+} porphyrin IX (heme) in the active site. The catalytic cycle of catalase involves a two-step reaction. In the first step, the enzyme (Fe^{3+} Por) in the resting state reduces a hydrogen peroxide molecule to water and generates a ferryl porphyrin with a porphyrin π-cation radical (Fe^{4+}═O $Por^{+\bullet}$), so-called compound I. In the second step, compound I oxidizes a second hydrogen peroxide molecule to molecular oxygen and water (eqs 1 and 2) (*2*, *3*).

$$\text{enzyme } (Fe^{3+}\ \text{Por}) + H_2O_2 \rightarrow \text{CpdI } (Fe^{4+}{=}O\ Por^{+\bullet}) + H_2O \quad (1)$$

$$\text{CpdI } (Fe^{4+}{=}O\ Por^{+\bullet}) + H_2O_2 \rightarrow \text{enzyme } (Fe^{3+}\ \text{Por}) + H_2O + O_2 \quad (2)$$

‡ The gene sequence of EKTA catalase (accession number AB266484) has been deposited in GenBank/EMBL/DDBJ. The atomic coordinates and structure factors for EKTA catalase (PDB entry 2J2M) have been deposited in Protein Data Bank.

* To whom correspondence should be addressed: Research Institute of Genome-based Biofactory, National Institute of Advanced Industrial Science and Technology, Tukisamu-Higashi, Toyohira-ku, Sapporo 062-8517, Japan. Phone: 81-11-857-8909. Fax: 81-11-857-8980. E-mail: i.yumoto@aist.go.jp.

§ National Institute of Advanced Industrial Science and Technology.

|| Present address: ROM Co., Ltd., Chuo-ku, Sapporo 064-0804, Japan.

⊥ Hokkaido Tokai University.

@ Hokkaido University.

10.1021/bi061519w CCC: $37.00
Published on Web 12/13/2006

The reactive intermediate compound I is also observed when organic peroxides are used as substrates, and the rate of formation of compound I decreases with an increase in the molecular size of the leaving group [for example, H− > CH_3− > $HOCH_2$− > CH_3CH_2− > $CH_3C(=O)$− > CH_3-$(CH_2)_2$− > $CH_3(CH_2)_3OOH$] (*2*). Moreover, compound I has the potential to oxidize short-chain alcohols such as methanol and ethanol. The reaction rate constant of catalase is dependent on the molecular size of the substrate (*2*). The X-ray crystal structure of bovine liver catalase (BLC)[1] revealed that the main channel that is accessible from the protein surface to the active site restricts substrate access because of steric hindrance and the hydrophobic nature of the channel (*4*).

The main channels of catalase are 25−55 Å in length from the protein surface to the heme (*5*−*8*). It has been reported that the main channel leads the substrate to the active site. It is thought that the narrow channel ∼0−15 Å above the heme restricts substrate accessibility to the heme (*5*). There have been two reports about the role of the highly conserved amino acid residues that constitute the narrow channel. Zamocky et al. reported that a mutation of Val^{111}, 8 Å from the heme, to smaller amino acid residues, such as Ala, reduces catalatic activity and enhances peroxidatic activity with large molecules as the substrate, presumably because of the reduction of selectivity for H_2O_2, and the side chains of these residues are critical for the construction of the bottleneck of the channel (*9*). Chelikani et al. (*10*) reported that the substitution of Asp^{181}, 12 Å from the heme, with Asn, Gln, Ala, Ser, or Ile reduces enzymatic activity except for Glu, because the potential field between negatively charged Asp (or Glu) and positively charged heme is important for enzymatic activity. Thus, the reactivity of catalase is strongly dependent on the nature of amino acid residues in the narrow channel. However, other sites or structures in the main channel and the relationship between the size of the bottleneck in the channel and the accessibility of the active site for substrates have not yet been elucidated. In this report, because of the presence of the bottleneck in the main access channel, we focus on the site 8−15 Å from the heme where amino acid residues are not conserved well in the main channel.

The dismutation reaction of hydrogen peroxide has evolved in at least three phylogenetically unrelated protein forms: monofunctional catalase, catalase-peroxidase (*11*, *12*), and non-heme catalase (*13*, *14*). Phylogenetic analysis based on the conserved core region of monofunctional catalases has revealed their subdivision into three distinct clades (*15*, *16*). Clade 1 catalases are mainly of plant origin and also include algal and bacterial catalases. Clade 2 catalases are large-subunit catalases of bacterial, archabacterial, and fungal origins. This clade of catalases exhibits a strong resistance to denaturation by heat and proteolysis (*17*). Clade 3 catalases are of bacterial, archabacterial, and eukaryotic origins. There is no pronounced functional difference between clade 3 and clade 1 catalases. The crystal structures of 11 monofunctional clade 1−3 catalases have been determined, and it has been shown that *Pseudomonas syringae* catalase (PSCF) (*18*) belongs to clade 1, *Penicillium vitale* catalase (PVC) (*19*), *Escherichia coli* catalase (HPII) (*6*, *20*), and *Neurospora crassa* catalase (NCC-1) (*8*) belong to clade 2, and bovine liver catalase (BLC) (*21*, *22*), *Micrococcus luteus* catalase (MLC) (*23*), *Proteus mirabilis* catalase (PMC) (*5*), *Saccharomyces cerevisiae* catalase (SCC-A) (*24*), human erythrocyte catalase (HEC) (*7*), *Helicobacter pylori* catalase (HPC) (*25*), and *Enterococcus faecalis* catalase (EFC) (*26*) belong to clade 3. In this study, we will show another example of the crystal structure of a clade 1 catalase.

There have been many reports of bacterial oxidative stress responses (*27*) but very few reports of microorganisms that can survive in highly oxidative environments. VktA catalase has been purified from *Vibrio rumiensis* S-1^T, which was isolated from a drain pool of a fish processing plant in which H_2O_2 is used (*28*). VktA catalase belongs to clade 3 (*29*). We also have isolated a new microorganism from environments with high concentrations of H_2O_2. *Exiguobacterium oxidotolerans* T-2-2^T, exhibiting a catalase activity without induction by oxidative stress, was isolated from a water sample collected from a drain pool of a fish processing plant in Hokkaido, Japan, in which H_2O_2 is used as a bleaching agent (*30*). The strain exhibits a high level of H_2O_2 resistance without stimulation by H_2O_2. The cell extract exhibits catalase activity of approximately 25 000 units/mg of protein, which is very high compared with the activities of catalases from conventional microorganisms. For example, the catalase activity of strain T-2-2^T is 558 times higher than that of *Es. coli*. In this report, we describe the reactivity of purified catalase from *E. oxidotolerans* (EKTA catalase) and the three-dimensional structure of this enzyme refined to a 2.4 Å resolution. EKTA catalase very rapidly reacted with organic peroxides compared with BLC and MLC. The results suggest that the difference between the rates of formation of compound I with organic peroxides of different molecular sizes depends on the size of the bottleneck of the main channel.

EXPERIMENTAL PROCEDURES

Chemicals. Standard chemicals were purchased from Wako Pure Chemicals. They were of the highest grade available and were used without further purification.

Methyl hydroperoxide was prepared by the method described by O'Sullivan et al. (*31*) with the modification described by Messer et al. (*32*). Peracetic acid was purchased from Sigma. Peracetic acid was treated with a trace amount of catalase (∼2 nM) in 50 mM potassium phosphate buffer (pH 7.0) before being used to eliminate hydrogen peroxide (*33*). The concentrations of peroxides were determined on the basis of the extinction coefficient (ϵ) at 353 nm of 2.62×10^4 M^{-1} cm^{-1} for triiodide by the oxidation of potassium iodide (*34*).

BLC purchased from Sigma (C-3155) was purified according to a previously reported method (*35*) with some modifications. One hundred milligrams of BLC was diluted in 20 mM Tris-HCl buffer (pH 8.0) and then absorbed onto an anion-exchange column (Q-Sepharose Fast Flow, 2.5 cm × 20 cm, Amersham Biosciences). Proteins were eluted with a buffered linear gradient of NaCl concentrations (from 0 to

[1] Abbreviations: EKTA catalase, *Exiguobacterium oxidotolerans* T-2-2^T catalase; BLC, bovine liver catalase; MLC, *Micrococcus luteus* catalase; PSCF, *Pseudomonas syringae* catalase; SDS−PAGE, sodium dodecyl sulfate−polyacrylamide gel electrophoresis; EPR, electron paramagnetic resonance.

0.25 M). Fractions containing catalase were collected and further purified by size exclusion chromatography (Sephacryl S-300 High Resolution, 1.6 cm × 60 cm, Pharmacia) with 50 mM potassium phosphate buffer (pH 7.0) containing 0.25 M NaCl. The purified enzyme that exhibited a 405 nm/280 nm absorbance ratio of 0.80 was stored at −30 °C until it was used. The catalase concentration was determined spectrophotometrically using 3.24×10^5 M^{-1} cm^{-1} as the molar extinction coefficient at 405 nm (*36*).

M. luteus catalase (MLC) purchased from Nagase ChemteX was purified according to a previously reported method (*37*) with slight modifications. Two grams of MLC was dissolved in 50 mM potassium phosphate buffer (pH 7.0) containing 1.0 M ammonium sulfate and then absorbed onto a hydrophobic interaction column (Phenyl Sepharose High Performance, 1.6 cm × 10 cm, Amersham Biosciences). Proteins were eluted with a buffered linear gradient of ammonium sulfate concentrations (from 1.0 to 0.4 M). Fractions exhibiting absorbance at 406 nm caused by catalase were collected and further purified by size exclusion chromatography (Sephacryl S-300 High Resolution, 1.6 cm × 60 cm) with 50 mM potassium phosphate buffer (pH 7.0) containing 0.25 M NaCl. The purified enzyme that exhibited a 406 nm/280 nm absorbance ratio of 0.93 was stored at −30 °C until it was used. The catalase concentration was determined spectrophotometrically using 4.12×10^5 M^{-1} cm^{-1} as the molar extinction coefficient at 405 nm (*38*).

Bacterial Strain. E. oxidotolerans T-2-2^T was cultivated aerobically up to the early stationary growth phase at 27 °C in PYS-2 medium (pH 7.5) containing (per liter of deionized water) 8.0 g of polypeptone (Nihon Pharmaceutical), 3.0 g of yeast extract (Kyokuto), and 5.0 g of NaCl. The organism was cultured in 15 L of the above-mentioned medium in a 20 L stainless-steel fermentor at an agitation speed of 100 rpm. Cells were harvested by centrifugation at 10000*g* for 20 min at 4 °C.

Purification of Catalase from E. oxidotolerans (EKTA Catalase). E. oxidotolerans T-2-2^T cells (approximately 25 g of wet cells) were suspended in 400 mL of 10 mM Tris-HCl buffer (pH 8.0) containing 1 mM EDTA and 10 μM phenylmethanesulfonyl fluoride (PMSF) (buffer A). Then 0.35 mg of lysozyme and 2000 units of DNase I were added to the suspension, which was gently stirred for 1 h at 25 °C. The lysis solution was passed through a French pressure cell (SLM-AMICO Instruments) at 18 000 lb/in.^{2} and centrifuged at 14000*g* for 30 min to remove unbroken cells. The resulting supernatant was recentrifuged at 105000*g* for 2 h to obtain the soluble fraction. The soluble fraction was diluted with buffer A and subjected to the first chromatography on a Q-Sepharose Fast Flow column (5 cm × 15 cm) equilibrated with buffer A. The enzyme was eluted with a linear gradient of NaCl concentrations (from 0 to 0.6 M) produced from 2 L of buffer A. The eluates containing catalase were combined and diluted with 10 mM Tris-HCl buffer (pH 8.0) and then subjected to a second chromatography on a Q-Sepharose Fast Flow column (2.5 cm × 20 cm) equilibrated with 10 mM Tris-HCl buffer (pH 8.0) containing 0.25 M NaCl (buffer B). The adsorbed enzyme was eluted with a linear gradient of NaCl concentrations (from 0.25 to 0.5 M) produced from 2 L of buffer B. The eluate was concentrated using Amicon Ultra-15 and then passed through a gel filtration column (Sephacryl S-300 High Resolution, 2.5 cm × 90 cm) equilibrated with buffer B. The protein content was determined by the bicinchoninic acid (BCA) method (*39*) using a BCA Protein Assay Reagent kit (PIERCE) with bovine serum albumin as a standard. The molar extinction coefficient of EKTA catalase at the Soret band was determined by the pyridine ferrohemochrome method on the basis of an extinction coefficient of 34.4 mM^{-1} cm^{-1} at 557 nm (*40*).

Molecular Weight Determination. The molecular masses of the subunits were determined by sodium dodecyl sulfate−polyacrylamide gel electrophoresis (SDS−PAGE) on a 10 to 20% gradient gel (PAGEL, ATTO) according to the method of Laemmli (*41*). The molecular weight standard of the BenchMark Protein Ladder was purchased from Invitrogen. The molecular weight of the native enzyme was determined by gel filtration using 7.8 mm × 300 mm × 2 columns, Protein PAK 300 (Waters), equilibrated with 0.1 M potassium phosphate buffer (pH 7.0). For molecular mass standards, the following proteins were used: thyroglobulin (669 kDa), apoferritin (443 kDa), α-amylase (200 kDa), alcohol dehydrogenase (150 kDa), bovine serum albumin (66.2 kDa), and carbonic anhydrase (29 kDa).

N-Terminal Amino Acid Sequencing. The purified EKTA catalase was analyzed on an HPLC system (Tosoh) with a YMC-Pack Pro C-4 reverse-phase column (4.6 mm × 100 mm) eluted at a flow rate of 0.8 mL/min with a gradient from 0.1% trifluoroacetic acid in water to 0.1% trifluoroacetic acid containing 80% acetonitrile in water over the course of 120 min. The eluent containing EKTA catalase was collected by monitoring the absorbance at 214 nm. The N-terminal amino acid sequence of EKTA catalase was analyzed on a protein sequencer (Applied Biosystems, model 491) by the Edman method.

Spectroscopy. Optical absorption spectra of purified proteins were recorded using a Cary 100 Bio spectrophotometer (Varian). Electron paramagnetic resonance (EPR) spectra of catalases were recorded using a Bruker ESP-300 instrument operating at 9.5 GHz. Experiments were carried out at a microwave power of 1 mW with a field modulation of 1 mT at 100 kHz. An Oxford flow cryostat (ESR-900) was used for liquid helium temperature measurements. The microwave frequency was monitored with a Hewlett-Packard 5350B frequency counter, and magnetic flux density was determined using a Bruker ER-035M NMR gaussmeter. The measurement of the resting state of EKTA catalase was carried out at 4 K in 50 mM potassium phosphate buffer (pH 7.0). The cyanide-binding form of the enzyme was prepared by reaction with 100 equiv of potassium cyanide, which was recorded at 10 K in 50 mM potassium phosphate buffer (pH 7.0). The concentration of each sample was 25 μM.

Catalase Activity and Kinetic Measurements. Catalase activity was measured spectrophotometrically by monitoring the decrease in absorbance at 240 nm resulting from the elimination of hydrogen peroxide, using a Unisoku RSP-1000 stopped-flow spectrophotometer. The concentration of hydrogen peroxide was determined on the basis of an extinction coefficient of 43.6 M^{-1} cm^{-1} at 240 nm (*42*). The reaction was recorded immediately after 1/1 mixing of 20 nM catalase and 60 mM hydrogen peroxide in 50 mM sodium phosphate buffer (pH 7.0) at 25 °C. The amount of enzyme activity that decomposed 1 μmol of hydrogen peroxide per minute was defined as 1 unit of activity.

The optical absorbance changes of EKTA catalase (final concentration of 1.7 μM) upon mixing with a small amount of excess methyl hydroperoxide (final concentration of 8.0 μM) were measured at 5 °C in 50 mM potassium phosphate buffer (pH 7.0). Spectral changes were monitored on a Unisoku RSP-1000 stopped-flow spectrophotometer.

The rate constant in the reaction of catalases with hydrogen peroxide was determined by measurement of the overall rate constant together with measurement of the steady-state proportion of the resting state and reactive intermediate (compound I) (*43*).

The reactions of catalases (final concentration of 0.5 μM) with methyl hydroperoxide, peracetic acid, and *tert*-butyl hydroperoxide were performed in 50 mM sodium phosphate buffer (pH 7.0) at 5 °C. Spectral changes in the Soret peak during compound I formation were recorded on a Unisoku RSP-1000 stopped-flow spectrophotometer. The kinetic constants were determined by varying the peroxide concentration under pseudo-first-order conditions.

The reaction rates of cyanide binding by catalases (final concentration of 1 μM) were measured in 50 mM potassium phosphate buffer (pH 7.0) at 25 °C. Spectral changes in the Soret peak during cyanide binding were recorded using a Unisoku RSP-1000 stopped-flow spectrophotometer. The kinetic constants were determined by varying the potassium cyanide concentration under pseudo-first-order conditions.

Cloning of Catalase Gene. Chromosomal DNA was isolated from *E. oxidotolerans* T-2-2^T according to the method of Marmur (*44*). To obtain the partial nucleotide sequence of EKTA catalase, two PCR primers were designed on the basis of the determined N-terminal amino acid sequence and conserved region of other homologues. Degenerate sense P-N1 5′-ATGAAYGARAAYGARAARAA-3′ and antisense P-S1 5′-TCSIRISTIGCRTGGTTRAA-3′ primers, where Y, R, S, and I represent A/T, A/G, C/G, and inosine, respectively, were used in PCR. An approximately 700 bp PCR fragment was successfully amplified, and the 693 bp DNA sequence was identified after subcloning into the pT7Blue T-vector (Novagen). Four PCR primers were designed by the inverse PCR method (*45*) from the internal DNA sequence of EKTA catalase (P-N3, 5′-GATGTTTGTC-CGTGGATCTGG-3′; P-N4, 5′-AGTGTGTACCATGAAT-GACGG-3′; P-S3, 5′-CGCTACTGGGATTTCATGACAC-3′; P-S4, 5′-CCGTAAAATGCGTGGTTCTTC-3′). Template DNA was prepared for digestion of the genomic DNA of *E. oxidotolerans* T-2-2^T with *Xba*I at 37 °C for 4 h, and then DNA fragments were cyclized by intramolecular ligation. A 4.5 kb DNA fragment was amplified in the first PCR using the P-N3−P-S3 primer set. The second PCR was carried out using the P-N4−P-S4 primer set to confirm whether the 4.5 kb PCR product contained the internal DNA sequence of EKTA catalase. The total 1546 bp DNA sequence, including the entire nucleotide sequence of EKTA catalase, was determined by sequencing of the PCR-amplified DNA.

Crystallization, Data Collection, and Refinement. The initial screening of crystallization conditions was performed by the sparse-matrix sampling method (*46*) using Crystal Screen (Hampton Research) and Wizard and Cryo Screens (DeCODE Genetics). Crystallization was performed using the hanging-drop vapor-diffusion method (*47*) at 293 K using a 24-well VDX plate (Hampton Research). The volume of a droplet, which consisted of equal volumes of EKTA catalase and reservoir solution, was 2 μL. The initial conditions under which crystals appeared were refined by varying the pH of the buffer and the concentration of the precipitant. The best crystals of EKTA catalase were grown from 100 mM MES buffer (pH 6.0), 12−13% (w/v) polyethylene glycol 10000, 5% (w/v) polyethylene glycol 400, and 20% (w/v) glycerol over a period of ~1 month. They were plate- or rod-shaped crystals approximately 0.5 mm × 0.3 mm × 0.1 mm in size.

Prior to data collection, a crystal was mounted on a loop made from a nylon fiber that was 20 μm in diameter and immersed in liquid nitrogen for freezing. Data from EKTA catalase were collected at 100 K on beamline NW12 of the Photon Factory, KEK, Japan, using an ADSC Quantum 4R CCD detector with 1.000 Å radiation and processed with HKL2000 (*48*) and the CCP4 program suite (Collaborative Computational Project, Number 4, 1994).

The structure of EKTA catalase was determined by a molecular replacement method with MOLREP (*49*) in the CCP4 package. The model coordinates were derived from the structure of bovine liver catalase (*50*) (PDB entry 8CAT). A rotation search using reflections having a resolution between 20 and 3.0 Å followed by a translation search gave a clear solution for the EKTA catalase structure.

Refinements of the structure of EKTA catalase were carried out using 20−2.4 Å intensity data with CNS (*50*) and REFMAC5 (*52*). Reflection data chosen randomly from 5.0% of the observed data were used for calculation of the free *R*-factor (*53*). The torsion angle of the main-chain atoms was analyzed in the Ramachandran plot produced using PROCHECK (*54*).

Molecular cavities were analyzed with VOIDOO using a reduced atomic radius of polar atoms (*55*).

RESULTS

Purification of Catalase from E. oxidotolerans T-2-2^T (EKTA catalase). A three-step purification procedure consisting of two steps of anion-exchange chromatography and one step of gel filtration chromatography was developed to obtain a purified catalase from *E. oxidotolerans* T-2-2^T (Table S1 of the Supporting Information). The procedure resulted in an approximately 15-fold purification with a 56% yield. The purified EKTA catalase exhibited a specific activity of 430 000 units/mg of protein at 25 °C in 50 mM sodium phosphate buffer (pH 7.0) containing 30 mM H_2O_2. SDS−PAGE of the purified EKTA catalase showed a single band at 64 kDa (Figure 1), and analytical gel filtration showed a molecular mass of 240 kDa for the native enzyme. The results indicate that the EKTA catalase is composed of four identical subunits.

Spectroscopy. The optical absorption spectra of the resting-state EKTA catalase and its cyanide derivative in 50 mM potassium phosphate buffer (pH 7.0) are shown in Figure 2. The absorption spectrum of resting-state EKTA catalase exhibited a Soret band at 408 nm with broad peaks at 506 and 627 nm. The Soret band at 408 nm is slightly different from absorbances at 405 nm in BLC and at 406 nm in MLC, and a resulting absorbance ratio of 408 nm to 280 nm of 1.36 is the highest among those of reported catalases. The molar extinction coefficient of EKTA catalase at 408 nm was determined to be 4.39×10^5 M^{-1} cm^{-1} on the basis of pyridine ferrohemochrome. The absorption spectrum of the

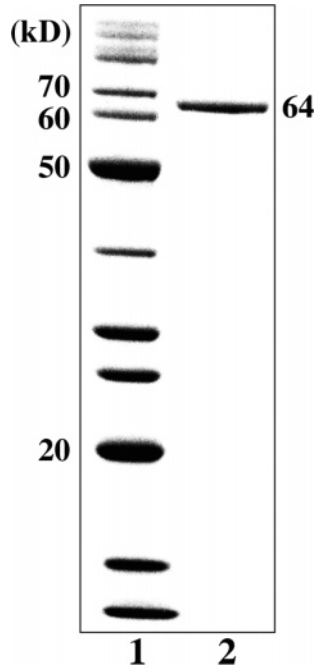

FIGURE 1: SDS−PAGE of EKTA catalase (lane 2) and protein marker (lane 1).

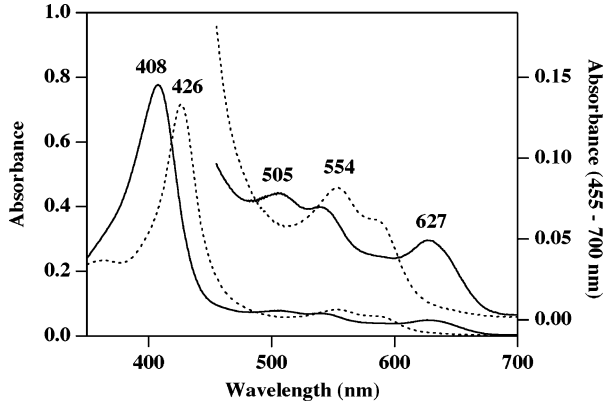

FIGURE 2: Electronic absorption spectra of resting-state (—) and cyanide-binding (···) forms of EKTA catalase in 50 mM potassium phosphate buffer (pH 7.0). The visible region starting at 455 nm is magnified, and the absorbance scale is given at the right.

cyanide-binding form exhibited two bands in the visible region at 554 nm with a shoulder at ~590 nm, and the intensity of the Soret band decreased and shifted to 426 nm.

Figure 3 shows the EPR spectra of resting-state EKTA catalase at 4 K and its cyanide derivatives at 10 K in 50 mM potassium phosphate buffer (pH 7.0). The EPR spectrum of resting-state EKTA catalase indicated a high-spin ferric state with rhombically split signals. The catalase exhibited the following g values: $g_x = 6.41$ ($g_x = 6.69$ as a minor component), $g_y = 5.36$, and $g_z = 1.97$. The cyanide-binding form of EKTA catalase exhibited three peaks with g values of 2.89, 2.22, and 1.59, similar to the g values of 2.84, 2.24, and 1.66, respectively, for human erythrocyte catalase (HEC) (*56*).

Stopped-Flow Experiments. To examine the formation rate of a reactive intermediate, compound I, the absorption spectral changes upon mixing EKTA catalase with methyl hydroperoxide in 50 mM phosphate buffer (pH 7.0) at 5 °C were observed using a stopped-flow rapid-scan spectrophotometer. Figure 4A shows the spectral changes during

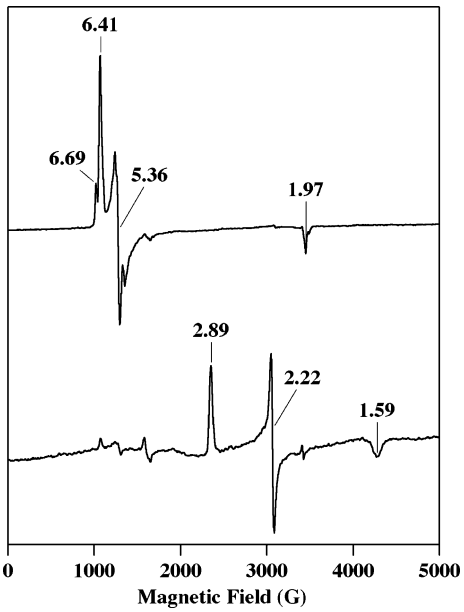

FIGURE 3: EPR spectra of resting-state (top) and cyanide-binding (bottom) forms of EKTA catalase. The resting-state and cyanide-binding forms of the enzyme were analyzed in 50 mM potassium phosphate buffer (pH 7.0) at 4 and 10 K, respectively. The protein concentration of each sample was 25 μM.

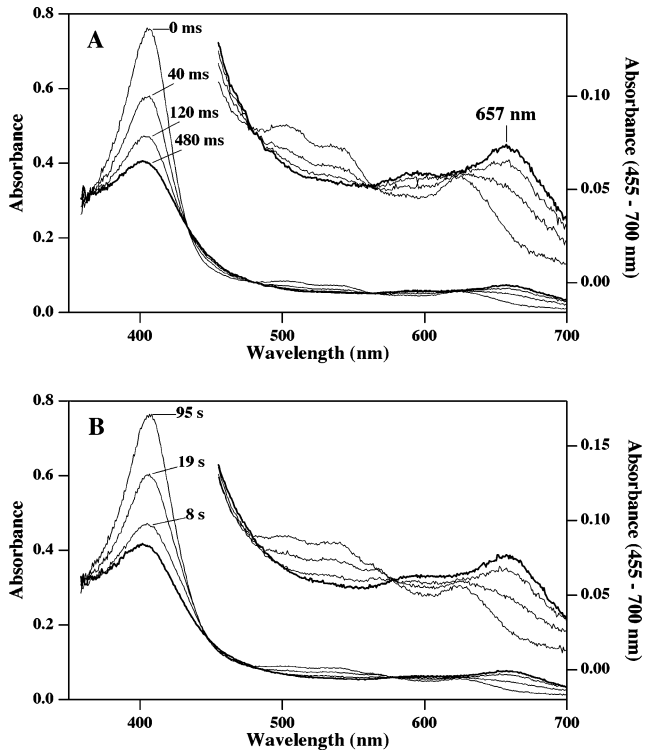

FIGURE 4: Rapid-scan spectra of EKTA catalase in its reaction with a small excess of methyl hydroperoxide during compound I formation (A) and spontaneous decay of compound I (B). The thick line represents the spectrum of compound I. The visible region starting at 455 nm is magnified, and the absorbance scale is given at the right.

compound I formation in the reaction of EKTA catalase with ~1.2 equiv amount of methyl hydroperoxide. The active form of the enzyme was estimated to be 94% from the absorbance change of 408 nm with 10 equiv of methyl hydroperoxide. The magnitude of the Soret peak of the resting-state EKTA catalase at 408 nm decreased after

Table 1: Comparison of Cyanide Binding and Compound I Formation Rates in the Reaction with Hydrogen Peroxide, Methyl Hydroperoxide, Peracetic Acid, and *tert*-Butyl Hydroperoxide

catalase	hydrogen peroxide ($\times 10^7$ M^{-1} s^{-1})	methyl hydroperoxide ($\times 10^4$ M^{-1} s^{-1})	peracetic acid ($\times 10^2$ M^{-1} s^{-1})	*tert*-butyl hydroperoxide ($\times 10^2$ M^{-1} s^{-1})	cyanide ($\times 10^6$ M^{-1} s^{-1})
EKTA	3.5	254 ± 2.9	5220 ± 49	182 ± 11	5.42 ± 0.11
BLC	1.1	20.8 ± 0.40	67.9 ± 1.4	16.5 ± 0.28	1.21 ± 0.033
MLC	3.4	6.76 ± 0.045	4.40 ± 0.097	2.54 ± 0.067	1.24 ± 0.045

compound I formation and shifted to 404 nm; a shift to 402 nm was observed in the reaction with 10 equiv of methyl hydroperoxide. In the visible region, the spectrum of compound I exhibited a peak at 657 nm with a broad shoulder at ~590 nm. Figure 4B shows the spectral changes during the spontaneous decay of compound I in the reaction with ~1.2 equiv of methyl hydroperoxide. Most of compound I directly returned to the resting state without conversion to compound II, which is a one-electron reduction product of compound I.

The formation rate constant of compound I for the reaction of EKTA catalase with hydrogen peroxide was slightly higher than that of MLC and 3 times higher than that of BLC (Table 1). The formation rates of compound I in the reactions with methyl hydroperoxide, peracetic acid, and *tert*-butyl hydroperoxide were determined by the rate of decrease in Soret peak intensity (Table 1). The rate of reaction of EKTA catalase with methyl hydroperoxide was approximately 12 times higher than that of BLC and 38 times higher than that of MLC; furthermore, EKTA catalase reacted 77 times faster than BLC and 1200 times faster than MLC in the reaction with peracetic acid, which as a molecule is sterically larger than methyl hydroperoxide. The rate of EKTA catalase reaction with *tert*-butyl hydroperoxide was 11 times higher than that of BLC and 72 times higher than that of MLC catalase. The binding rate constant of cyanide in 50 mM phosphate buffer (pH 7.0) at 25 °C was 5 times higher than those of BLC and MLC (Table 1). The rate constants of the binding reactions of hydrogen peroxide with EKTA, MLC, and BLC were almost the same in the pH range of 6.0−9.0, whereas the rates fluctuated depending on the catalase at pH <6 (Figure S1 of the Supporting Information).

Nucleotide Sequence of EKTA Catalase. The total 1546 bp DNA sequence that includes the entire nucleotide sequence of EKTA catalase was determined. The deduced amino acid sequence showed that EKTA catalase is composed of 491 amino acids with a calculated molecular mass of 56 487.7 Da (Figure 5). In a search of the protein database, sequence similarities were found between the predicted ORF product and known catalases. The sequence similarity values were 69, 67, 67, 63, and 63% for catalases from *Listeria seeligeri*, *Listeria monocytogenes*, *Listeria innocua*, *Bacillus anthracis*, and *Bacillus cereus*, respectively. EKTA catalase was categorized into clade 1 according to its amino acid sequence. Figure 5 shows a sequence alignment of BLC, MLC, and EKTA catalase. A comparison of catalase sequences revealed that the amino acid residues important for enzyme activity are well-conserved (Figure 5).

Crystal Structure of EKTA Catalase. The EKTA catalase crystal belongs to monoclinic space group $P2_1$, with the following unit cell parameters: $a = 94.3$ Å, $b = 131.9$ Å, $c = 110.6$ Å, and $\beta = 107.6°$. On the basis of the estimated V_M value (*57*), the asymmetric unit was assumed to contain one EKTA catalase tetramer giving a V_M of 3.1 $Å^3$/Da and

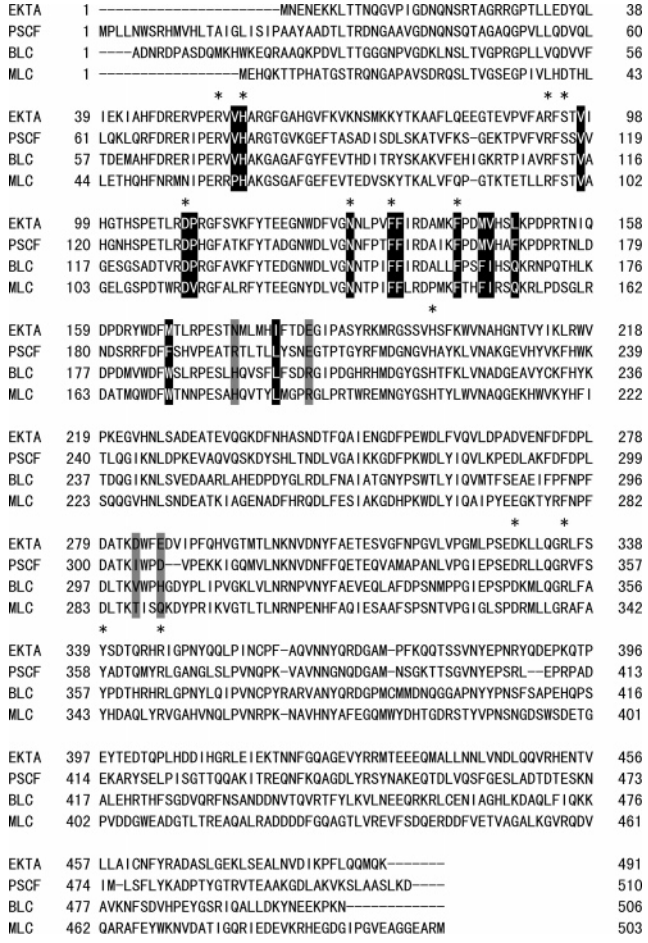

FIGURE 5: Sequence alignment of EKTA catalase, PSCF, BLC, and MLC. The amino acid residues involved in the narrow channel are highlighted in black. The residues important for NADPH binding are highlighted in gray. The residues important for enzyme activity are indicated by statistics.

a solvent content of approximately 61%. Diffraction intensities from the crystal were collected to 2.4 Å with an R_{merge} of 0.049 and a completeness of 99.0%. Table 2 summarizes statistics of data collection and refinement. The crystallographic and free *R*-factors were 0.199 and 0.230, respectively. The model of EKTA catalase has 16 284 non-H atoms corresponding to the tetramer of EKTA catalase, four hemes, and 536 solvent molecules. The rms deviations from the standard values (*58*) of the bond length and angles were 0.013 Å and 1.43°, respectively. A Ramachandran plot showed that most residues fell into the most favored regions (89.0%), additional allowed regions (10.5%), and generously allowed regions (0.2%). Only 0.2% of the molecules fell into the disallowed regions. The deviation of Cα atoms in a superposition of EKTA catalase with PSCF, BLC, and MLC results in root-mean-square deviations of 1.05, 1.02, and 1.10 Å, respectively. The structures of side-chain atoms of 480 amino acids were identified from Lys^6 to Phe^{485} in each

Table 2: Statistics for Data Collection and Refinement of EKTA Catalase[a]

data collection	
beamline	PF NW12
wavelength (Å)	1.000
resolution (Å)	2.4
R_{merge}[b]	0.049 (0.060)
no. of observed reflections	329160
no. of independent reflections	99632
completeness (%)	99.0 (97.8)
multiplicity	3.3 (2.7)
$\langle I/\sigma(I)\rangle$	11.6 (10.4)
refinement statistics	
resolution range (Å)	20−2.4
R-factor[c]	0.199 (0.201)
free *R*-factor	0.230 (0.257)
rmsd for bond lengths (Å)	0.013
rmsd for bond angles (deg)	1.43
Ramachandran plot (%)	
residues in most favored regions	89.0
residues in additional allowed regions	10.5
residues in generously allowed regions	0.2
residues in disallowed regions	0.2
average *B*-factor (Å^2)	15.6

[a] Values in parentheses are for the highest-resolution shell (2.53−2.4 Å). [b] $R_{merge} = \sum\sum_j|\langle I(h)\rangle - I(h)_j|/\sum\sum_j\langle I(h)\rangle$, where $\langle I(h)\rangle$ is the mean intensity of a set of equivalent reflections. [c] *R*-factor $= \sum||F_{obs}(h)| - |F_{calc}(h)||/\sum|F_{obs}(h)|$, where F_{obs} and F_{calc} are the observed and calculated structure factors, respectively.

subunit where the electron density was unclear in the N-terminal and C-terminal regions. A stereoview of EKTA catalase and an electron density map of the main channel are shown in Figure 6. The side-chain structures of amino acids were identical to the predicted amino acid sequence deduced from the DNA sequence. The structure of the heme environment was similar to those of other catalases as had been suggested by sequence alignment. For example, as assigned in BLC, essential His[56] and Asn[129], the hydrogen bond between His[56] and Ser[95], the axial ligand of Tyr[339] to the heme iron with a hydrogen bond network of Arg[335], His[199], and Asp[329], the aromatic stacking of Phe[134] and Phe[142] to the heme, and the salt bridge formation of heme propionates with Arg[53], Arg[93], and Arg[346] (EKTA catalase numbering) were conserved in PSCF, BLC, MLC, and EKTA catalase (Figure 5). The superimposed structures of EKTA catalase and PSCF revealed that the tertiary structures of conserved amino acid residues around the heme were also identical to each other (data not shown). However, the size of the bottleneck of the main channel of EKTA catalase was larger than that of PSCF (Figure 7). The heme group orientation is similar to those of PSCF, HPII, and NCC-1, where the imidazole group of distal His[56] is stacked parallel to pyrrole ring IV. It seems that Val[198], which is near pyrrole ring I, regulates heme orientation, probably because of the steric hindrance between the methyl group of Val[198] and the vinyl group of pyrrole ring II. An electron density map showed no significant density in the region corresponding to the NADPH-binding site. The crystal structure of PSCF also exihibited no electron density for NADPH. An analysis of the NADPH-binding site for clade 3 catalases suggests that the His[193]-Arg[202]-Val[301]-His[304] (BLC numbering) sequence is important for NADPH binding. The equivalent sequences in PSCF and EKTA catalase are Arg[196]-Glu[205]-Ile[304]-Asp[307] and Asn[175]-Glu[184]-Asp[283]-Glu[286], respectively.

Structure of the Main Channel. The main channel of catalase permits access of the substrate from the protein surface to the active site and plays a role in selection of substrates (*7*). The narrow channel, the lower part of the channel between heme and conserved Asp[127], comprises 14 residues: Val[73], His[74], Val[115], Asp[127], Pro[128], Asn[147], Phe[152], Phe[153], Phe[160], Phe[163], Ile[164], Gln[167], Trp[185], and Leu[198] in BLC (Figure 7). This combination is typical among catalases. The results of sequence alignment for 432 catalases revealed that the combination of the first nine residues [Val[73] (80%)-His[74] (99%)-Val[115] (95%)-Asp[127] (97%)-Pro[128] (54%)-Asn[147] (97%)-Phe[152] (99%)-Phe[153] (94%)-Phe[160] (99%) (numbering based on BLC)] is highly conserved in all catalases (% indicates conservation ratio). In contrast, the latter combination [Phe[163] (35%)-Ile[164] (50%)-Gln[167] (30%)-Trp[185] (30%)-Leu[198] (64%) (numbering based on BLC)] is less conserved. In EKTA catalase, the latter combination was as follows: Met[145] (20%)-Val[146] (32%)-Leu[149] (22%)-Met[167] (2.6%)-Ile[180] (2.3%). Met[167] and Ile[180] are rarely placed at the entrance of the narrow channel. The position at Met[167] is normally occupied by aromatic amino acid residues such as tryptophan or phenylalanine. The combination of the first four residues, Met[145]-Val[146]-Leu[149]-Met[167] (numbering based on EKTA catalase), is employed only in *B. cereus* (*59*), *B. anthracis* (*60*), and *Bacillus thuringensis* (GenBank/EMBL/DDBJ accession number AE017355 for the sequence) as compared with those of other known catalases. However, their catalytic characteristics have not yet been reported. Atom-to-atom distances of key amino acid residues for formation of bottleneck 15 Å from heme were estimated (Table S2 of the Supporting Information). The distances between Leu[149] and Ile[180] and between Asp[109] and Met[167] in the bottleneck 15 Å from the iron in the main channel of EKTA catalase are 7.22 and 9.11 Å, respectively. These values are much larger than those of BLC and MLC. The Leu[149]−Ile[180] and Asp[109]−Met[167] combinations at the entrance of the narrow channel in the main channel determine the size of the bottleneck. The narrow channel of MLC was similar to that of BLC except for Pro[60] and Val[114]. Figure 7 shows cavity structures determined by using a 1.2 Å radius probe in BLC, MLC, and EKTA catalase. The Trp residues (i.e., Trp[185] in BLC and Trp[171] in MLC) placed at the entrance of the narrow channel seem to constrict the main substrate channel. On the other hand, a large space exists at the entrance of the narrow channel as a result of the replacement of the Trp residue with Met[167] in EKTA catalase. The distance between the entrance of the narrow channel and heme iron is ∼14−15 Å. The diameters estimated by the smallest probe not able to access the narrow channel are ∼2.7 Å for EKTA catalase, ∼2.3 Å for BLC, and ∼2.1 Å for MLC.

DISCUSSION

In this study, EKTA catalase was characterized and its crystal structure was determined. The calculated molecular mass of this catalase (56 487.7 Da) is similar to those of other clade 1 and 3 catalases (55−69 kDa). The deviation of Cα atoms in the superposition of EKTA catalase with PSCF, BLC, and MLC results in root-mean-square deviations of 1.05, 1.02, and 1.10 Å, respectively. The results indicate that the subunit structure of EKTA catalase is similar to those of other catalases. Moreover, the heme group orientation and the lack of a NADPH-binding site are common in the

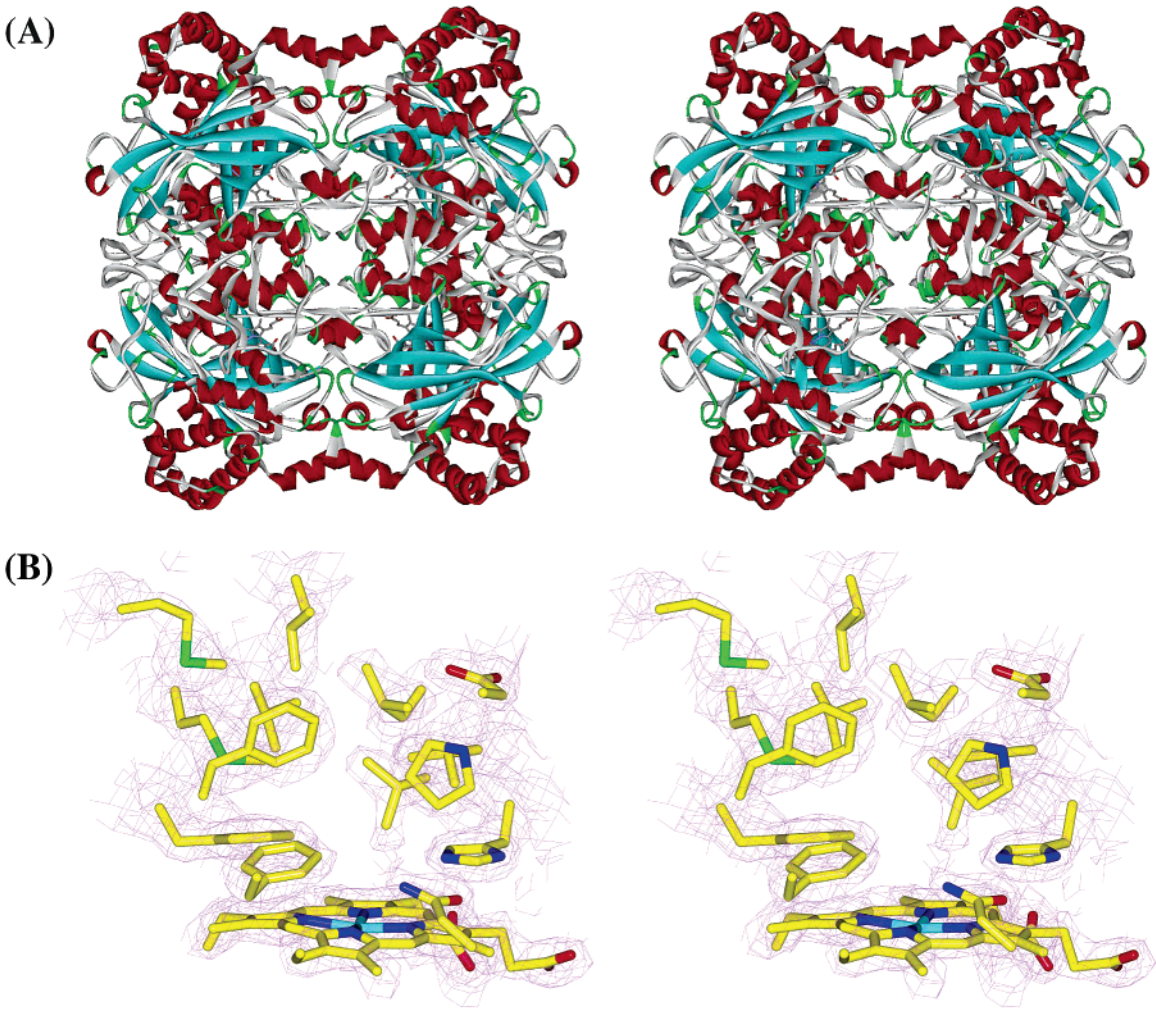

FIGURE 6: Structure of EKTA catalase. (A) Stereoview of the overall structure of EKTA catalase. Colors are placed according to the secondary structure. Helices are colored red, β-sheets cyan, turns green, and coils white. (B) Stereoview of the structure of the main channel with the electron density map on critical residues. The $2F_o - F_c$ density is modeled at 1.5σ.

structures of clade 1 and clade 2 catalases (*17*). The amino acid sequence deduced from the nucleotide sequence of the catalase exhibited a high degree of similarity with those of clade 1 catalases, and the catalase was determined to belong to clade 1 in the phylogenetic tree on the basis of the sequence (Figure S2 of the Supporting Information).

Most of compound I directly returned to the resting state of EKTA catalase without conversion to compound II. However, it is thought that a small amount of compound II was formed because there was no clean isosbestic point at ~480 nm during the return to the resting state (Figure 4). The prevention of inactive compound II formation is known to involve NADPH in clade 3 catalases (*61*, *62*), but the mechanism by which this is achieved remains unclear (*61*−*64*). The covalent bonds of proximal Tyr^{415} with His^{392} and Tyr^{379} with Cys^{356} in HPII (*65*) and NCC-1 (*8*), respectively, which are categorized as clade 2 catalases, could make the enzyme resistant to inactivation by H_2O_2. However, EKTA catalase does not bind NADPH due to the absence of the binding sequence (His^{193}-Arg^{202}-Val^{301}-His^{304} in BLC) in the structure, and no post-translational modification of the proximal tyrosine has been observed. Hence, it is most likely that binding of NADPH and modification of the proximal tyrosine are not necessary in EKTA catalase. The fact that EKTA catalase was transformed to an equivalent amount of compound I corresponding to the amount of organic peroxide that reacted means that compound I is very stable because the formation and reduction rates of compound I were 2.54×10^6 and 3000 M^{-1} s^{-1}, respectively.

The binding rate constant of cyanide with EKTA catalase was 5 times higher than those of cyanide with BLC and MLC. Cyanide is mostly protonated at pH 7 because the pK_a of HCN is approximately 9, and the crucial step for cyanide association has been shown to be the deprotonation of HCN in the distal heme pocket as suggested for the binding of H_2O_2 (pK_a = 11.6) (*66*). Also, HCN must transit the main substrate channel in catalase for binding to the heme iron. Thus, it is thought that at least three factors, namely, the deprotonation rate constant, the rate of entering the main channel, and the suitability of the substrate of the main channel structure for the reaction, are important for definition of the reaction rate of binding of cyanide to heme iron. The amino acids around the heme in BLC and EKTA catalase are the same, and the main channel structure in these catalases may be constructed for suitability for the reaction with H_2O_2 but not with HCN. The possible effect of ionizable residues in the main channel in the vicinity of the active site less likely occurs at the pH for this measurement. The highest binding rate for cyanide in EKTA catalase among the three catalases may be due to a decrease in steric

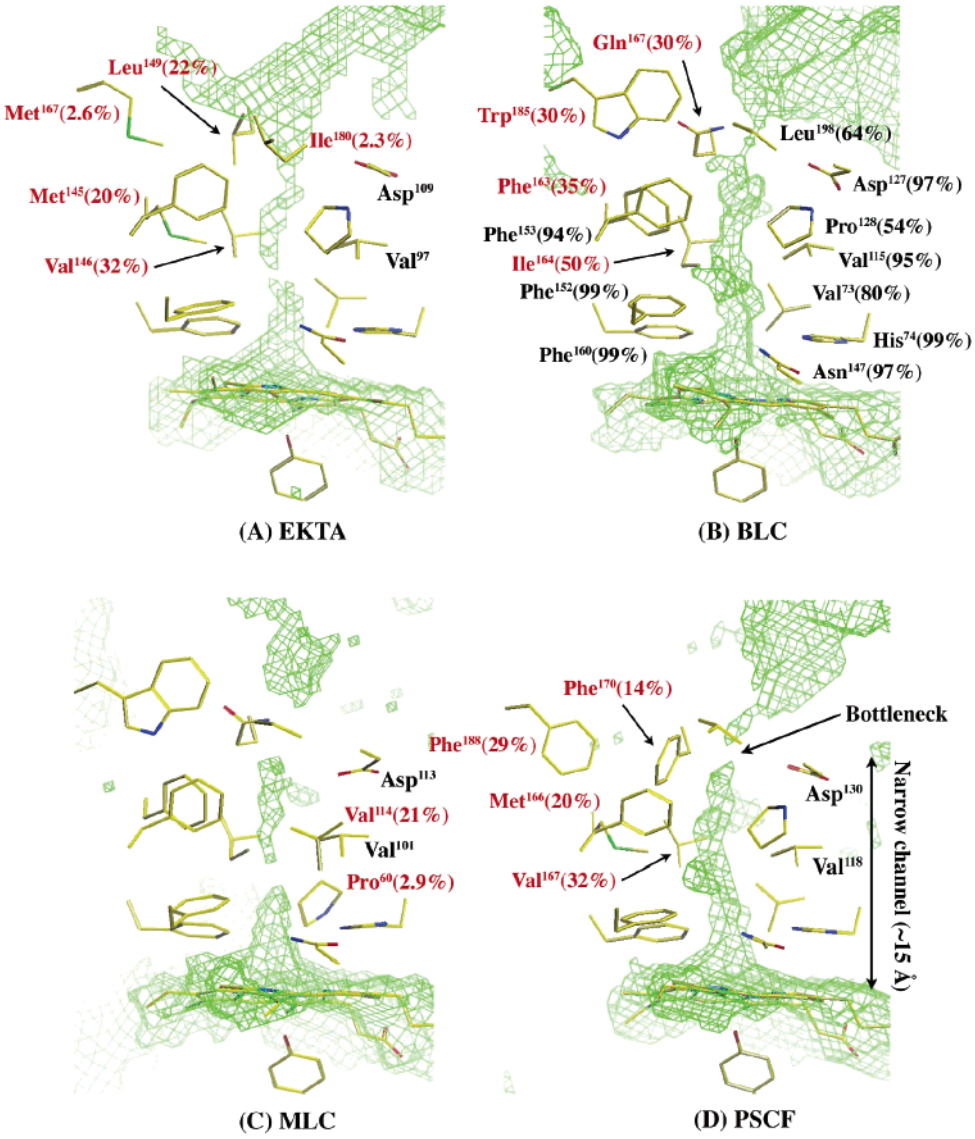

FIGURE 7: Structures of main channels of EKTA catalase (A), BLC (B), MLC (C), and PSCF (D). The accessible surfaces are represented as green lattices. The percentage in parentheses indicates the possibility of a residue being in its corresponding place in the database based on the nucleotide sequence of catalase. Residues of EKTA catalase, MLC, and PSCF different from those of BLC are shown in red (A, C, D). Red labels in BLC denote residues with a low likelihood (≤50) of being in the corresponding places in the database.

hindrance of the main channel, since it is unlikely that there are pronounced differences in other factors.

Recently, the three-dimensional shape and size of the main channel have been suggested to regulate the enzymatic efficiency of catalases (*7*, *17*, *18*). The long and narrow channel appears to preorient and select preferred substrates. The residues lining hydrophobic side chains constrict the distal channel to 2−3 Å. This structure allows only H_2O, H_2O_2, or other small molecules to enter (*7*). The short occupancy time within the hydrophobic site of H_2O and the impossibility of forming a H_2O-H_2O hydrogen bond in the channel structure make H_2O_2 a more preferable substance in the channel than H_2O for catalase (*7*). The rate of formation of compound I in the reaction with organic peroxide decreases with an increase in the molecular size of the leaving group. In fact, human erythrocyte catalase (HEC) reacts with methyl hydroperoxide 100 times faster than it does with peracetic acid (*67*). This result was confirmed in this work using BLC and MLC. The formation rates of compound I in the reaction with peracetic acid were ~30 and ~150 times lower than those in the reaction with methyl hydroperoxide for BLC and MLC, respectively. On the other hand, the reaction rate of EKTA catalase with peracetic acid was 5 times lower than that with methyl hydroperoxide. Furthermore, EKTA catalase reacted with peracetic acid 77 times faster than did BLC and 1200 times faster than did MLC, and a second-order rate constant of 5.22×10^5 M^{-1} s^{-1} in the reaction of compound I formation with peracetic acid is the highest among those of reported catalases (*68*). The results suggest that the narrow channel of EKTA catalase has an enlarged structure for accepting molecules larger than hydrogen peroxide. The diameters of the bottleneck 15 Å from the iron (the entrance of the narrow channel) in the main channel estimated from the minimum probe radius required to disrupt the channel are ~2.7 Å for EKTA catalase, ~2.3 Å for BLC, and ~2.1 Å for MLC. Since the cross section at the bottleneck in the main channel is proportional to the square of the radius, the cross section at the bottleneck for EKTA catalase is the largest among those of the three catalases. The reaction rate constant of each

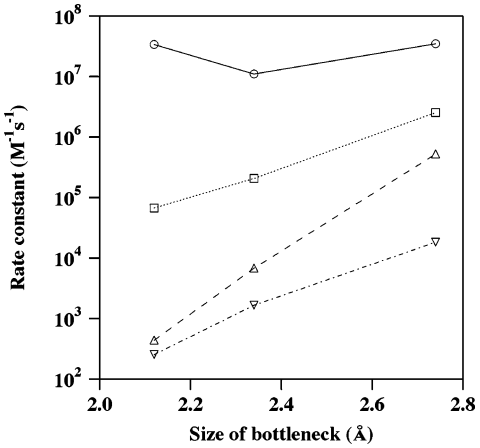

FIGURE 8: Relationship between the rate of compound I formation and the size of the bottleneck in the main channel. EKTA catalase, BLC, and MLC were used: (○) hydrogen peroxide, (□) methyl hydroperoxide, (△) peracetic acid, and (▽) *tert*-butyl hydroperoxide.

catalase decreased with an increase in the molecular size of the substrates, and catalase with a larger-sized bottleneck 15 Å from the iron in the main channel exhibited a lower rate of reduction in the compound I formation rate with an increase in the molecular size of substrates. Furthermore, the rate constants of catalase reactions were directly proportional to the size of the bottleneck in the main channel in the reaction with substrates larger than H_2O_2 (Figure 8). These findings indicate that the size of the bottleneck of the main channel is an important factor for the reaction rate constant corresponding to the size of the substrate. The results described above indicate that EKTA catalase rapidly reacts with organic peroxides to enhance accessibility of molecules larger than hydrogen peroxide molecules to the active site by an enlarged structure at the bottleneck of the main channel.

Although the major portion of the narrow channel comprises highly conserved amino acid residues, there is also a partial structure comprising diverse amino acid combinations. This region is not thought to play a major role in the catalytic reaction because of the distance (8−15 Å) from the active site and the diversity of amino acid residues. The Leu[149]−Ile[180] and Asp[109]−Met[167] combinations at the bottleneck of the main channel in EKTA catalase are rarely found in other catalases (compared with more than 432 catalase genes in the gene database). It has been thought that the optimization of the main channel structure for the appropriate reaction of catalase involves several factors such as the position of hydrophobic amino acid residues, the molecular ruler effect, the interaction between charged residues and heme, the molecular motion of the side chain of amino acids, and the position of H_2O molecules. Therefore, it seems difficult to ascribe the relationship between the characteristics of catalase reaction and the corresponding basis of the structure to only a single amino acid. Alterations of either smaller (V169A) or larger (V169I) residues reduce enzyme-specific activity in HPII (*17*). Furthermore, an increase in the size of bottleneck of the main channel of EKTA catalase may cause a reduction in substrate selectivity. However, the reactivity of the bottleneck in EKTA catalase with H_2O_2 is thought to be very high because of its high catalytic reaction rate. The Leu[149]−Ile[180] and Asp[109]−Met[167] combinations have an important meaning for the determination of the size of the bottleneck 15 Å from the iron in the main channel.

There is a possibility that the interruption of the access of substrates larger than H_2O_2 at a narrow channel other than the site described above in the main channel near the active site occurs in catalase. The rational mutation of Val[111] to Ala in *S. cerevisiae* catalase (SCC-A) to enlarge the narrow channel increases peroxidatic activity by increasing the accessibility of large molecules (*9*). The steric hindrance by Val[97] in EKTA catalase, comparable to Val[111] in SCC-A, could inhibit the access of large molecules. Nevertheless, EKTA catalase exhibited a rapid reaction with peracetic acid. This result suggests that when the substrate comes into the narrow channel, the substrate could reach the active site. Therefore, it is thought that the cross section at the entrance of the bottleneck 15 Å from the iron is important for the reaction with large molecules.

In this study, the size of the bottleneck 15 Å from the iron (the entrance of the narrow channel) in the main access channel of catalase was shown to be an important factor for the determination of the rate of formation of compound I when a molecule larger than H_2O_2 is the substrate. The first 20 Å of the main channel starting from the surface of the protein is funnel-shaped, presenting little obstacle to even large molecule. On the other hand, the next 15 Å of the channel (narrow channel) extending from a conserved Asp[127] (BLC numbering) to heme is constricted, restricting access to only small molecules (*69*). It is thought that a certain motion of side chains contained in the narrow channel is indispensable for substrate access in the reaction of catalases because the van der Waals radius of an oxygen atom is ∼1.5 Å; i.e., the diameter is ∼3.0 Å. It thus appears that the mobility of the side chain surrounding the narrow channel is probably the most important feature dictating substrate access, and the size of the bottleneck identified in this work may be an important factor that defines the accessibility of a substrate due to the location of the bottleneck at the entrance of the narrow channel.

SUPPORTING INFORMATION AVAILABLE

Purification of catalase from *E. oxidotolerans* T-2-2[T] (Table S1), diameters of the bottleneck 15 Å from iron and atom-to-atom distances of key amino acid residues (Table S2), pH dependence of the rate of compound I formation in the reaction with hydrogen peroxide for catalases (Figure S1), and phylogenetic tree based on amino acid sequences of 22 catalases constructed via the neighbor-joining method (Figure S2). This material is available free of charge via the Internet at http://pubs.acs.org.

REFERENCES

1. Chance, B., Sies, H., and Boveris, A. (1979) Hydroperoxide metabolism in mammalian organs, *Physiol. Rev. 59*, 527−605.
2. Schonbaum, G. R., and Chance, B. (1976) Catalase, in *The enzymes* (Boyer, P. D., Ed.) pp 363−408, Academic Press, New York.
3. Deisseroth, A., and Dounce, A. L. (1970) Catalase: Physical and chemical properties, mechanism of catalysis, and physiological role, *Physiol. Rev. 50*, 319−375.
4. Fita, I., and Rossmann, M. G. (1985) The active center of catalase, *J. Mol. Biol. 185*, 21−37.
5. Gouet, P., Jouve, H. M., and Dideberg, O. (1995) Crystal structure of *Proteus mirabilis* PR catalase with and without bound NADPH, *J. Mol. Biol. 249*, 933−954.

6. Bravo, J., Mate, M. J., Schneider, T., Switala, J., Wilson, K., Loewen, P. C., and Fita, I. (1999) Structure of catalase HPII from *Escherichia coli* at 1.9 Å resolution, *Proteins 34*, 155−166.
7. Putnam, C. D., Arvai, A. S., Bourne, Y., and Tainer, J. A. (2000) Active and inhibited human catalase structures: Ligand and NADPH binding and catalytic mechanism, *J. Mol. Biol. 296*, 295−309.
8. Diaz, A., Horjales, E., Rudino-Pinera, E., Arreola, R., and Hansberg, W. (2004) Unusual Cys-Tyr covalent bond in a large catalase, *J. Mol. Biol. 342*, 971−985.
9. Zamocky, M., Herzog, C., Nykyri, L. M., and Koller, F. (1995) Site-directed mutagenesis of the lower parts of the major substrate channel of yeast catalase A leads to highly increased peroxidatic activity, *FEBS Lett. 367*, 241−245.
10. Chelikani, P., Carpena, X., Fita, I., and Loewen, P. C. (2003) An electrical potential in the access channel of catalases enhances catalysis, *J. Biol. Chem. 278*, 31290−31296.
11. Claiborne, A., and Fridovich, I. (1979) Purification of the *o*-dianisidine peroxidase from *Escherichia coli* B. Physicochemical characterization and analysis of its dual catalatic and peroxidatic activities, *J. Biol. Chem. 254*, 4245−4252.
12. Hochman, A., and Shemesh, A. (1987) Purification and characterization of a catalase-peroxidase from the photosynthetic bacterium *Rhodopseudomonas capsulata*, *J. Biol. Chem. 262*, 6871−6876.
13. Kono, Y., and Fridovich, I. (1983) Isolation and characterization of the pseudocatalase of *Lactobacillus plantarum*, *J. Biol. Chem. 258*, 6015−6019.
14. Allgood, G. S., and Perry, J. J. (1986) Characterization of a manganese-containing catalase from the obligate thermophile *Thermoleophilum album*, *J. Bacteriol. 168*, 563−567.
15. Klotz, M. G., Klassen, G. R., and Loewen, P. C. (1997) Phylogenetic relationships among prokaryotic and eukaryotic catalases, *Mol. Biol. Evol. 14*, 951−958.
16. Nicholls, P., Fita, I., and Loewen, P. C. (2001) Enzymology and structure of catalases, *Adv. Inorg. Chem. 51*, 51−106.
17. Chelikani, P., Fita, I., and Loewen, P. C. (2004) Diversity of structure and properties among catalases, *Cell. Mol. Life Sci. 61*, 192−208.
18. Carpena, X., Soriano, M., Klotz, M. G., Duckworth, H. W., Donald, L. J., Melik-Adamyan, W., Fita, I., and Loewen, P. C. (2003) Structure of the clade 1 catalase, catF of *Pseudomonas syringae*, at 1.8 Å resolution, *Proteins 50*, 423−436.
19. Vainshtein, B. K., Melik-Adamyan, W. R., Barynin, V. V., Vagin, A. A., Grebenko, A. I., Borisov, V. V., Bartels, K. S., Fita, I., and Rossmann, M. G. (1986) Three-dimensional structure of catalase from *Penicillium vitale* at 2.0 Å resolution, *J. Mol. Biol. 188*, 49−61.
20. Bravo, J., Verdaguer, N., Tormo, J., Betzel, C., Switala, J., Loewen, P. C., and Fita, I. (1995) Crystal structure of catalase HPII from *Escherichia coli*, *Structure 3*, 491−502.
21. Murthy, M. R., Reid, T. J., III, Sicignano, A., Tanaka, N., and Rossmann, M. G. (1981) Structure of beef liver catalase, *J. Mol. Biol. 152*, 465−499.
22. Reid, T. J., III, Murthy, M. R., Sicignano, A., Tanaka, N., Musick, W. D., and Rossmann, M. G. (1981) Structure and heme environment of beef liver catalase at 2.5 Å resolution, *Proc. Natl. Acad. Sci. U.S.A. 78*, 4767−4771.
23. Murshudov, G. N., Melik-Adamyan, W. R., Grebenko, A. I., Barynin, V. V., Vagin, A. A., Vainshtein, B. K., Dauter, Z., and Wilson, K. S. (1992) Three-dimensional structure of catalase from *Micrococcus lysodeikticus* at 1.5 Å resolution, *FEBS Lett. 312*, 127−131.
24. Mate, M. J., Zamocky, M., Nykyri, L. M., Herzog, C., Alzari, P. M., Betzel, C., Koller, F., and Fita, I. (1999) Structure of catalase-A from *Saccharomyces cerevisiae*, *J. Mol. Biol. 286*, 135−149.
25. Loewen, P. C., Carpena, X., Rovira, C., Ivancich, A., Perez-Luque, R., Haas, R., Odenbreit, S., Nicholls, P., and Fita, I. (2004) Structure of *Helicobacter pylori* catalase, with and without formic acid bound, at 1.6 Å resolution, *Biochemistry 43*, 3089−3103.
26. Hakansson, K. O., Brugna, M., and Tasse, L. (2004) The three-dimensional structure of catalase from *Enterococcus faecalis*, *Acta Crystallogr. D60*, 1374−1380.
27. Farr, S. B., and Kogoma, T. (1991) Oxidative stress responses in *Escherichia coli* and *Salmonella typhimurium*, *Microbiol. Rev. 55*, 561−585.
28. Yumoto, I., Ichihashi, D., Iwata, H., Istokovics, A., Ichise, N., Matsuyama, H., Okuyama, H., and Kawasaki, K. (2000) Purification and characterization of a catalase from the facultatively psychrophilic bacterium *Vibrio rumoiensis* S-1^T exhibiting high catalase activity, *J. Bacteriol. 182*, 1903−1909.
29. Ichise, N., Morita, N., Kawasaki, K., Yumoto, I., and Okuyama, H. (2000) Gene cloning and expression of the catalase from the hydrogen peroxide-resistant bacterium *Vibrio rumoiensis* S-1 and its subcellular localization, *J. Biosci. Bioeng. 90*, 530−534.
30. Yumoto, I., Hishinuma-Narisawa, M., Hirota, K., Shingyo, T., Takebe, F., Nodasaka, Y., Matsuyama, H., and Hara, I. (2004) *Exiguobacterium oxidotolerans* sp. nov., a novel alkaliphile exhibiting high catalase activity, *Int. J. Syst. Evol. Microbiol. 54*, 2013−2017.
31. O'Sullivan, D. W., Lee, M. Y., Noone, B. C., and Heikes, B. G. (1996) Henry's law constant determinations for hydrogen peroxide, methyl hydroperoxide, hydroxymethyl hydroperoxide, ethyl hydroperoxide, and peroxyacetic acid, *J. Phys. Chem. 100*, 3241−3247.
32. Messer, B. M., Stielstra, D. E., Cappa, C. D., Scholtens, K. W., and Elrod, M. J. (2000) Computational and experimental studies of chemical ionization mass spectrometric detection techniques for atmospherically relevant peroxides, *Int. J. Mass Spectrom. 197*, 219−235.
33. Jones, P., and Middlemiss, D. N. (1972) Formation of compound I by the reaction of catalase with peroxoacetic acid, *Biochem. J. 130*, 411−415.
34. Ramette, R. W., and Sandford, R. W. (1965) Thermodynamics of iodine solubility and triiodide ion formation in water and in deuterium oxide, *J. Am. Chem. Soc. 87*, 5001−5005.
35. Torii, K., and Ogura, Y. (1969) Electron paramagnetic resonance study of bovine liver catalase, *J. Biochem. 65*, 825−827.
36. Samejima, T., and Yang, J. T. (1963) Reconstitution of acid-denatured catalase, *J. Biol. Chem. 238*, 3256−3261.
37. Jones, P., Pain, R. H., and Suggett, A. (1970) Dissociation of catalase. A correlation between changes in sedimentation and spectroscopic properties accompanying dissociation of bacterial catalase in alkaline solution, *Biochem. J. 118*, 319−323.
38. Brill, A. S., and Williams, R. J. P. (1961) Primary compounds of catalase and peroxidase, *Biochem. J. 78*, 253−262.
39. Smith, P. K., Krohn, R. I., Hermanson, G. T., Mallia, A. K., Gartner, F. H., Provenzano, M. D., Fujimoto, E. K., Goeke, N. M., Olson, B. J., and Klenk, D. C. (1985) Measurement of protein using bicinchoninic acid, *Anal. Biochem. 150*, 76−85.
40. De Duve, C. A. (1948) Spectrophotometric method for the simultaneous determination of myoglobin and hemoglobin in extracts of human muscle, *Acta Chem. Scand. 2*, 264−289.
41. Laemmli, U. K. (1970) Cleavage of structural proteins during the assembly of the head of bacteriophage T4, *Nature 227*, 680−685.
42. Hildebraunt, A. G., and Roots, I. (1975) Reduced nicotinamide adenine dinucleotide phosphate (NADPH)-dependent formation and breakdown of hydrogen peroxide during mixed function oxidation reactions in liver microsomes, *Arch. Biochem. Biophys. 171*, 385−397.
43. Chance, B. (1952) Effect of pH upon the reaction kinetics of the enzyme-substrate compounds of catalase, *J. Biol. Chem. 194*, 471−481.
44. Marmur, J. (1961) A procedure for the isolation of deoxyribonucleic acid from micro-organisms, *J. Mol. Biol. 3*, 208−218.
45. Ochman, H., Gerber, A. S., and Hartl, D. L. (1988) Genetic applications of an inverse polymerase chain reaction, *Genetics 120*, 621−623.
46. Jancarik, J., Scott, W. G., Milligan, D. L., Koshland, D. E., Jr., and Kim, S. H. (1991) Crystallization and preliminary X-ray diffraction study of the ligand-binding domain of the bacterial chemotaxis-mediating aspartate receptor of *Salmonella typhimurium*, *J. Mol. Biol. 221*, 31−34.
47. McPherson, A. (1990) Current approaches to macromolecular crystallization, *Eur. J. Biochem. 189*, 1−23.
48. Otwinowski, Z., and Minor, W. (1997) Processing of X-ray diffraction data collected in oscillation mode, *Methods Enzymol. 276*, 307−326.
49. Vagin, A., and Teplyakov, A. (1997) Molrep: An automated program for molecular replacement, *J. Appl. Crystallogr. 30*, 1022−1025.
50. Fita, I., and Rossmann, M. G. (1985) The NADPH binding site on beef liver catalase, *Proc. Natl. Acad. Sci. U.S.A. 82*, 1604−1608.
51. Brunger, A. T., Adams, P. D., Clore, G. M., DeLano, W. L., Gros, P., Grosse-Kunstleve, R. W., Jiang, J. S., Kuszewski, J., Nilges,

M., Pannu, N. S., Read, R. J., Rice, L. M., Simonson, T., and Warren, G. L. (1998) Crystallography & NMR system: A new software suite for macromolecular structure determination, *Acta Crystallogr. D54*, 905−921.
52. Murshudov, G. N., Vagin, A. A., and Dodson, E. J. (1997) Refinement of macromolecular structures by the maximum-likelihood method, *Acta Crystallogr. D53*, 240−255.
53. Brunger, A. T. (1992) Free R-value: A novel statistical quantity for assessing the accuracy of crystal-structures, *Nature 355*, 472−475.
54. Laskowski, R. A., Macarthur, M. W., Moss, D. S., and Thornton, J. M. (1993) Procheck: A program to check the stereochemical quality of protein structures, *J. Appl. Crystallogr. 26*, 283−291.
55. Williams, M. A., Goodfellow, J. M., and Thornton, J. M. (1994) Buried waters and internal cavities in monomeric proteins, *Protein Sci. 3*, 1224−1235.
56. Palcic, M., and Dunford, H. B. (1979) Spectral studies of human erythrocyte catalase, *Can. J. Biochem. 57*, 321−329.
57. Matthews, B. W. (1968) Solvent content of protein crystals, *J. Mol. Biol. 33*, 491−497.
58. Engh, R. A., and Huber, R. (1991) Accurate bond and angle parameters for X-ray protein-structure refinement, *Acta Crystallogr. A47*, 392−400.
59. Ivanova, N., Sorokin, A., Anderson, I., Galleron, N., Candelon, B., Kapatral, V., Bhattacharyya, A., Reznik, G., Mikhailova, N., Lapidus, A., Chu, L., Mazur, M., Goltsman, E., Larsen, N., D'Souza, M., Walunas, T., Grechkin, Y., Pusch, G., Haselkorn, R., Fonstein, M., Ehrlich, S. D., Overbeek, R., and Kyrpides, N. (2003) Genome sequence of *Bacillus cereus* and comparative analysis with *Bacillus anthracis*, *Nature 423*, 87−91.
60. Read, T. D., Peterson, S. N., Tourasse, N., Baillie, L. W., Paulsen, I. T., Nelson, K. E., Tettelin, H., Fouts, D. E., Eisen, J. A., Gill, S. R., Holtzapple, E. K., Okstad, O. A., Helgason, E., Rilstone, J., Wu, M., Kolonay, J. F., Beanan, M. J., Dodson, R. J., Brinkac, L. M., Gwinn, M., DeBoy, R. T., Madpu, R., Daugherty, S. C., Durkin, A. S., Haft, D. H., Nelson, W. C., Peterson, J. D., Pop, M., Khouri, H. M., Radune, D., Benton, J. L., Mahamoud, Y., Jiang, L., Hance, I. R., Weidman, J. F., Berry, K. J., Plaut, R. D., Wolf, A. M., Watkins, K. L., Nierman, W. C., Hazen, A., Cline, R., Redmond, C., Thwaite, J. E., White, O., Salzberg, S. L., Thomason, B., Friedlander, A. M., Koehler, T. M., Hanna, P. C., Kolsto, A. B., and Fraser, C. M. (2003) The genome sequence of *Bacillus anthracis* ames and comparison to closely related bacteria, *Nature 423*, 81−86.
61. Hillar, A., and Nicholls, P. (1992) A mechanism for NADPH inhibition of catalase compound II formation, *FEBS Lett. 314*, 179−182.
62. Kirkman, H. N., Rolfo, M., Ferraris, A. M., and Gaetani, G. F. (1999) Mechanisms of protection of catalase by NADPH. Kinetics and stoichiometry, *J. Biol. Chem. 274*, 13908−13914.
63. Olson, L. P., and Bruice, T. C. (1995) Electron tunneling and ab initio calculations related to the one-electron oxidation of NAD(P)H bound to catalase, *Biochemistry 34*, 7335−7347.
64. Almarsson, O., Sinha, A., Gopinath, E., and Bruice, T. C. (1993) Mechanism of one-electron oxidation of NAD(P)H and function of NADPH bound to catalase, *J. Am. Chem. Soc. 115*, 7093−7102.
65. Bravo, J., Fita, I., Ferrer, J. C., Ens, W., Hillar, A., Switala, J., and Loewen, P. C. (1997) Identification of a novel bond between a histidine and the essential tyrosine in catalase HPII of *Escherichia coli*, *Protein Sci. 6*, 1016−1023.
66. Brancaccio, A., Cutruzzola, F., Allocatelli, C. T., Brunori, M., Smerdon, S. J., Wilkinson, A. J., Dou, Y., Keenan, D., Ikeda-Saito, M., Brantley, R. E., Jr., and Olson, J. S. (1994) Structural factors governing azide and cyanide binding to mammalian metmyoglobins, *J. Biol. Chem. 269*, 13843−13853.
67. Palcic, M. M., and Dunford, H. B. (1980) The reaction of human erythrocyte catalase with hydroperoxides to form compound I, *J. Biol. Chem. 255*, 6128−6132.
68. Dunford, H. B. (1999) *Heme peroxidases*, pp 435−453, Wiley-VCH, New York.
69. Switala, J., and Loewen, P. C. (2002) Diversity of properties among catalases, *Arch. Biochem. Biophys. 401*, 145−154.

BI061519W